Modeling of a Hawkmoth-Inspired Flapping Wing Micro Aerial Vehicle

Nida Tuz Zohra*
Wichita State University, Wichita, Kansas, 67208

The modeling of flapping flight dynamics consists of a multi-body system that is nonlinear and time-varying. An aerodynamic model is required along with control laws, flight dynamics and actuation mechanism. A review of the existing models in current literature is performed. A simple analytical model is used to describe the aerodynamics with leading edge vortex and rotational lift being the major contributors. This model calculates the aerodynamic loads and moments acting on the vehicle. Then, the longitudnal flight dynamics are computed using these loads and moments with vertical displacement and velocity, and flapping anlge and rate as the states. The aerodynamics and flight dynamics are modeled in Simulink using the characteristic parameters of a Hawkmoth. The model is actuated using an input torque that governs the flapping angle and rate. The results produced show that the input torque can be maniplulated to acheive ascend, descend and hover. Flight can be improved by including active pitch control instead of using passive pitching. As the system grows more complex, adaptive controllers can prove to be more efficient.

I. Nomenclature

α_m	=	mean angle of attack
$\overline{c}$	=	mean chord length
$C_{L\alpha}$	=	three dimensional lift curve slope
$\hat{d}$	=	distance between the wing root hinge point and the wing's center of gravity
η	=	pitching angle of the body
I_x, I_y, I_z	=	moment of inertia about x, y and z axis
I_{yb}	=	moment of inertia about the y_b axis
m	=	total mass
m_b	=	mass of the body and wing
m_w	=	mass of the wing
ϕ	=	flapping angle of the wing
ψ	=	yaw angle
R	=	wing radius
r_{cg}	=	distance between the wing root hinge point and the wing's center of gravity
ρ	=	air density
τ_ϕ	=	input torque
θ	=	plunging angle

II. Introduction

In an attempt to optimize flight vehicles, Unmanned Aerial Vehicles (UAV) have been developed with specific objectives. There are several subcategories of UAVs, one of them being micro aerial vehicles that use flapping flight called Flapping Wing Micro Aerial Vehicles (FWMAVs). DARPA (Defense adavanced Research Projects Agency) has set the span of Micro Aerial Vehicles (MAV) at 15cm and they are generally smaller than UAVs but bigger than NAVs (Nano Aerial Vehicles) and, typically, autonomous. The idea behind developing FWMAVs is to mimic nature, which allows for sophisticated biological surveillance. Apart from biological, military survellaince can also make use of MAVs given the small size and inconspicuous appearance.

*Graduate Student, Aerospace Engineering, 1845 N Fairmount St.

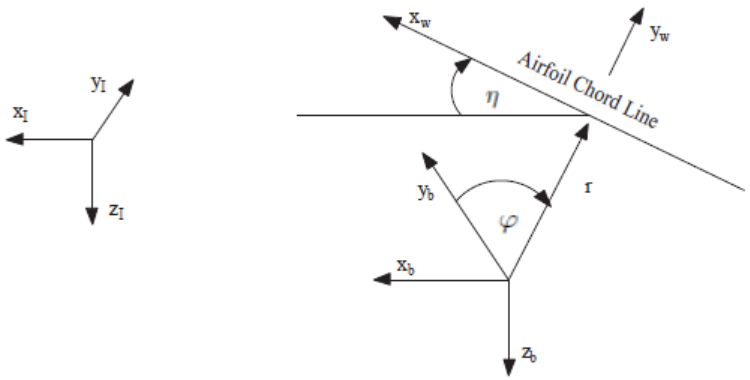

Fig. 1 The three fixed axis systems of FWMAV[1].

The general model of FWMAV consists of two parts; the flight dynamics which includes kinematics, aerodynamic modeling and equations of motion, and the control laws which establish the actuation mechanism. The flapping kinematics are governed by the Euler angles of the wing with respect to the body. The flapping angle is denoted by ϕ, plunging angle by θ and pitching angle of the body by η. Figure 1 shows the three fixed axis used to formulate the flight dynamics problem of FWMAV. In the figure, x_I, y_I and z_I represents the inertially fixed frame, x_b, y_b and z_b is the body-fixed frame and x_w, y_w and z_w is the wing-fixed frame and, r represents the position vector of the origin of the wing-fixed frame with respect to the origin of the body fixed frame. In the body-fixed frame y_b points to the right wing, x_b points in the direction of the forward velocity and z_b is perpendicular to the two axes. This body-fixed frame can be related to the inertial frame through any sequence of Euler angles. In order to get zero wing kinematic angles, the body-fixed frame and wing-fixed frame are made to coincide. Hence, the sequence of ϕ- θ- η, i.e., flapping-plunging-pitching is used to describe the wing-fixed frame with respect to body-fixed frame. In this project, a hawkmoth inspired vehicle is designed to demonstrate insect flight. The flapping kinematics are established using the equations of motion, followed by the calculation of forces and moments acting on the vehicle. These aerodynamic loads and moments are used to simulate the insect flight in different flight modes.

The objective of the kinematics is to manipulate the velocity vector with respect to the airfoil. Then the dynamic equations of motions defining the aerodynamic loads are written in the body-fixed frame. The lift and drag are calculated with respect to body fixed frame. The dynamic equations of a FWMAV are the same as that of a conventional aircraft are shown in Equations 1-6 and the kinematic equations are shown in Equations 7-9 where the derivatives of the body Euler angles ψ, θ and ϕ (yaw, pitch, flapping) govern the kinematics.

$$m(\dot{u} + qw - rv + g\sin\theta) = X \tag{1}$$
$$m(\dot{v} + ru - pw + g\sin\phi\cos\theta) = Y \tag{2}$$
$$m(\dot{w} + pv - qu + g\sin\phi\cos\theta) = Z \tag{3}$$
$$I_x\dot{p} - I_{xz}\dot{(r)} + (I_x - I_y)qr_w - I_{xz}pq = L \tag{4}$$
$$I_y\dot{q} + (I_x - I_z)r_w p + I_{xz}(p^2 - r_w^2) = M \tag{5}$$
$$I_z\dot{r_w} - I_{xz}\dot{(p)} + (I_y - I_x)pq + I_{xz}r_w q = N \tag{6}$$

$$\dot{\psi} = (q\sin\phi + r\cos\phi)/\cos\theta \tag{7}$$
$$\dot{\theta} = q\cos\phi - r\sin\phi \tag{8}$$
$$\dot{\phi} = p + (q\sin\phi + r\cos\phi)\tan\theta \tag{9}$$

A. Flapping Kinematics

There are three general configurations of flapping kinematics of FWMAVs. The first kind of cofiguration assumes harmonic functions which simplifies the analysis and in the second, the kinematics are inspired from insects and the third kinematic configurations are designed for specific manauevering purposes. In [2], Wang et. al tests different flapping wing shapes to find the optimal configuration with harmonic kinematics. Quasi steady aerodynamic modeling is used with varying wing shape parameter and the results show that fully actuated harmonic kinematics can be very efficient. Kinematic configuration, inspired from nature, is examined in depth in [3]. In ornithopter flight there are two degrees of freedom whereas insect flight requires three degrees of freedom; the flapping wing motion, the change in the stroke plane angle and wing rotation. Insect wing kinematics, as studied in [3] by Abas et. al, are of two different types: water treading and hovering. The 3D insect flight is extended from the 2D bird flight kinematic problem.

The third configuration where the kinematics are designed for specific control purposes is reviewed by Taha [1]. To acheive high control authority, Schenato et. al in [4] hovering kinematics with specific paramterization is proposed. The flapping angle is set using a constant angular velocity. Each wing is equipped with an actuator to control the flapping angle. For maximum lift, passive pitching is utilised and the angle of attack is maintained at 45°. The kinematic equation is described in Eq. 10.

$$\phi(t) = \begin{cases} A_0(1+\kappa)(1-\frac{2t}{\rho T}) + \gamma A_0, & 0 \leq t \leq \rho T \\ A_0(1+\kappa)(2\frac{t-\rho T}{(1-\rho)T} - 1) + \gamma A_0, & \rho T \leq t \leq T \end{cases} \tag{10}$$

In the above equation, γA_0 represents a bias, κ controls the amplitude of the motion and ρ is the downstroke duration relative to the whole cycle. Hence, γ, κ and ρ are the three kinematic parameters that can be controlled. If ρ = 1/2 then symmetric flapping is performed. However, asymmetric flapping is desired to generate thrust on both wings causing yawing moments. Using a quasi steady aerodynamic model, the loads and moments are linearized and then related to the kinematic parameters. A linear map, which is assumed to be a control effectiveness matrix, is created from the six kinematic parameters. The linear map between the the kinematic parameters for both wings and aerodynamic loads is shown in Eq. 11.

$$w_1 = -sinc(\frac{A_0}{4})[(\rho_{LW} - \frac{1}{2}) + (\rho_{RW} - \frac{1}{2})] \tag{11}$$

$$w_2 = \kappa_{LW} + \kappa_{RW}$$

$$w_3 = -sinc(\frac{A_0}{4})[\kappa_{LW} - \kappa_{RW}]$$

$$w_4 = -sinc(\frac{A_0}{4}[\gamma_{LW} + \gamma_{RW}]$$

$$w_5 = (\rho_{LW} - \frac{1}{2}) - (\rho_{RW} - \frac{1}{2})$$

It is noteworthy that the amplitude changes the vertical lift force w_2, i.e., κ must not be zero. A rolling moment, w_3, can be generated if κ_{LW} and κ_{RW} are not equal, i.e., the amplitude change on the two wings is asymmetric. Forward thrust, w_1, can be produced if there's any change in speed between the upstroke and downstroke, i.e. ρ_{LW} must not equal to ρ_{RW}. The pitching moment, denoted by w_4, can be produced by creating an offset which would shift the center of pressure of the aerodynamic forces longitudnally. The rank for the control effectiveness matrix corresponds to the number of controllable degrees of freedom. The linear map has a rank of five, which means the results showed that all the degrees of freedom were controlled except for the translation in the side force direction. It was proved that the nonlinear system, when linearized, is controllable about hover. Similar to Schenato et. al in [4], Doman et. al in [5] has one actuator per wing and generates maximum lift by maintaining the angle of attack at 45° by using passive pitching to prove the importance of minimal actuation. In [5] the vehicle used for investigation is the Robofly that uses piezoelectric actuators. It is controlled by varying the velocity profile of the wing strokes, hence the kinematic functions are based on the flapping angle of the vehicle. As in [4], Doman et. al in [5] create a linear map from the linearised dynamics about hover. The simulations showed that the controller performed well for the unsteady aerodynamics with minimal actuation.

To design a controller for multiple flight modes, Taha in [1] introduces the concept of Central Pattern Generators (CPGs). As defined by Hopper in [6], CPGs are "neural networks that can produce rhythmic patterned outputs without rhythmic sensory or central input." The controller is not responsible to produce the specific pattern to drive the degrees of freedom. Instead, the controller sets the frequency, amplitude and relative phase of the pattern, in turn reducing the complexity of the signal generated from it. Chung and Dorothy [7] used Hopf oscillator as the CPG model for two reasons: symmetry property and smooth bifurcation. The symmetry property helps in stabilising and smooth bifurcation is used to switch smoothly from flapping to gliding flight.

B. Aerodynamic Modeling

To model insect flight accurately, an aerodynamic modelis required which calculates the forces and moments such as lift and rolling moments, respectively. The most common method of formulating an aerodynamic model is through performing experiements, and then data fitting the results to form an approximate relation that describe the aerodynamic loads. As mentioned in [1], the model designed by Holst and Kuchemann in [8] is considered one of the first complete models. In this model, it was proven that maximal thrust is acheived a the phase difference between pitch and plunge angles of 90°. During early research of flapping wing models, quasi steady aerodynamics were used which is applicable to slow flapping large birds in forward flight. Another noteworthy discovery is the phenomenon of Leading Edge Vortex (LEV) which was discussed in [9] by Ellington et. al. A hawkmoth was placed in a wind tunnel for observation. The observations made the existence of vortices clear. The phenomenon was further studied by creating a 3D mechanical model of a hawkmoth with corresponding dimensions. Then, smoke was released from the leading edge of the wing as it flapped, which showed vortices being formed at the beginning of the downstroke. These vortices then detach from the wing after the middle of the downstroke. LEV causes a high-lift force and is a result of dynamic stall.

The most common aerodynamic models used for FWMAVs are quasi-steady. In [11], Khan and Agarwal present quasi-steady aerodynamic model for a wing that has a flapping and pitching angle, but zero out-of-plane stroke angle. To develop the model, translatory effects, rotational lift and added mass effects were considered while the viscous effects were assumed negligible. They were successfully able to create a model that can be used to determine aerodynamic loads and moments. Another quasi steady aerodynamic model is by Dickinson et. al [10], where the the model wing was allowed to move with a constant velocity at a particular angle of attack and the aerodynamic forces were recorded. In order to obtain greater lift, insects also make use of two other mechanisms called rotational lift and wake-capture effects as discussed in [10]. An experiment performed in which a dynamically scaled model of the fruit fly is built and a force sensor is added to the base of one wing that measures the aerodynamic forces over time. Both wings are capable of rotational motion about three axes. The results showed two rotational force peaks at two separate times. The force peak at the end of each half stroke is caused by the wing's own rotation called rotational lift, while the larger force peak is caused by the mechanism of wake capture, wherein the vortex shedding of the wing produces a negative lift in turn benefiting the wing at the appropriate angle. The last model is a quasi-steady aerodynamic model based on blade element theory by Wang et. al [12]. It considers LEV, rotational effect along with added mass effect like the Dickinson et. al [10] model but also includes viscous effects. The experiment is set up in a quasi 2-d flow with freely falling plates. Navier-Stokes equations are used to compare the results with numerical solutions. The results showed that there is a rotational term proportional to angular velocity of the fluttering and tumbling plates that dominates the fluid circulation.

C. Dynamic Stability

To derive equations of motion of flight dynamics of FWMAVs, generally, three important assumptions are made. Firstly, the wing intertial effects are assumed to be negligible. In systems where the wing mass is much smaller than body mass, it is reasonable to ignore wing inertial effects. This reduces the order resulting in a less complex system. In [13] a quasi steady aerodynamic model is used to compare the results of simulation when the wing mass is varied. The full wing mass is initially set to 5.7% of the body mass. It showed that when zero wing mass is used, the results are close to that of a standard aircraft. However, examining the results while varying wing mass as one-eigth of the wing mass, one-half of the wing- mass and full wing mass produced results that moved progressively farther from the desired outcome. It has been found that there exists a difference in the flight dynamics model behavior when the wing mass is as low as 0.7% of the body mass. Hence, it is important to take the wing mass in consideration while performing stability and control analysis.

To make the system autonomous, body dynamics is averaged over the flapping cycle. The second assumption made to derive the equations of motion is that averaging does not have any undesirable effects on the final body dynamics. Generally, the flight dynamics of a FWMAV can be converted to an autonmous system using the averaging theorem. In

[14], Nayfeh and Mook test several different mechanical structures by exciting the structures with a low amplitude and high frequency. The structures experimented with include cantilever beam, three arm frame and a composite plate. Considering the example of the metallic cantilever beam which was slightly bent, it was excited at a high frequency of 32.50 Hz. This resulted in the activation of the first mode response with a large amplitude which is of additive nature. Thus, the articles concludes that an excitation of low-amplitude, high-frequency can produce large amplitude responses which would produce erroneous results by adding over every cycle.

The third assumption is that linearizing the non-linear dynamic model gives a well-rounded model. There are two methods discussed in [1] to linearise the flight dynamics system. One method is to convert the nonlinear time periodic system (NLTP) to a nonlinear time invariant system (NLTI). This NLTI can then be linearised to a linear time invariant (LTI) whose stability analysis can be performed by simple matrix operations. The second method is to use the Floquet theory to perform stability analysis of the linearised time periodic system. In [15], the quasi-steady aerodynamic model from Dickinson et. al [10] is used along with nonlinear flight dynamics with six degrees of freedom of rigid body and several flexibile DOFs. The stability analysis was performed using Floquet theory. The results obtained showed unstable longitudnal modes and lateral modes. It has also been found that wing inertia caused a destabilizing effect on the subsidence modes by studying the loci of the eigenvalues.

D. Control Design

There are two approaches to control FWMAV as discussed in [16] by Zhang: linear and non-linear design. In [17], Schenato et. al develop a biomimetic insect model using standard aircraft aerodynamic model and time averaged forces and moments. It is controlled using a switching controller and is successfully operated in hover. In [18], Schenato et. al developed a flight control system for a flapping wing micromechanical flying insect. The flight dynamics is assumed to be NLTI system which is then linearized to discrete time LTI system. Using Linear Quadratic Regulator theorem, a LQR controller is created which was tested on a nonlinear, time-varying model. Stabilization was successfully acheived with a steady-state error of less than 5° for orientation.

Nonlinear control design is desirable to create robust systems. In [19], Serrani et. al developed a robust controller for a 3-DOF MAV model in hover. A case study is performed where the MAV moves simultaneously in both x and z direction from a set initial point. The results show that without an initial error in pitch angle, the x trajectory converges to its trim condition quickly. The controller is able to maintain the trajectory of a periodic orbit asymptotically stable about a given point. Another example of nonlinear controller design is the adaptive controller applied to RoboBee in [20]. Chirarattananon et. al in [20] developed an adaptive controller with the purpose of coping with modeling uncertainities and nonlinear systems. The controller successfully engages hover as well as vertical takeoff and landing but with a time delay of 0.2s. However, the time delay does not have any negative effects on stability. It is concluded that, compared to non adaptive controllers, adaptive controllers result in fewer position errors. MAVs with a fuzzy neural network controller have the advantage of being highly manuevrable. In [21] Guo et. al implement an insect-like FWMAV model with averaged flight dynamics, a fuzzy neural network controller. The results showed that the controller was able to robustly control the attitude and position making the vehicle highly maneuverable.

E. Actuation Mechanism

It is desirable for FWMAVs to utilise minimal actuation and one of the common ways to acheive it is by using smart materials like piezoelectric motors. However, to execute complex mechanisms such as active pitch control an equally complex driving mechanism amy be required. In [22], Balta, et. al review actuation mehcanisms of four different models that are popularly known. The first model is one developed by Hu and Deng in [23], referred to as the Purdue mechanism in [22], in which a $2.61 gram$ flapping wing vehicle is actuated by a dc drive

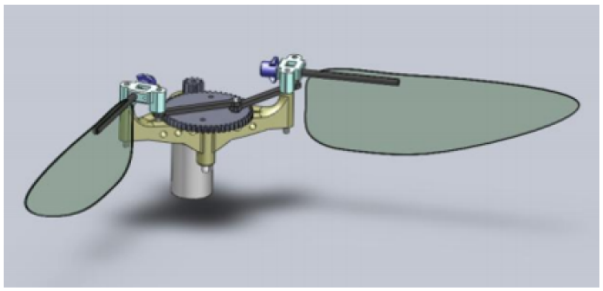

Fig. 2 Driving Mechanism developed by Hu and Deng [23]

(a) AeroVironment gears setup

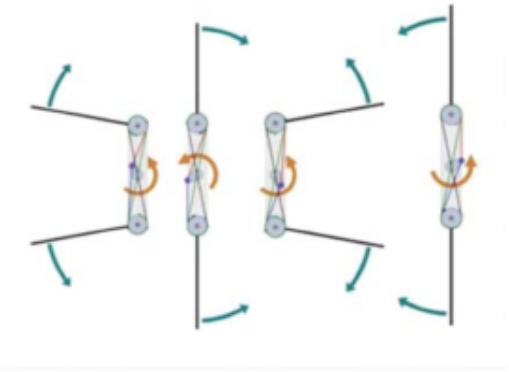

(b) Flapping wing mechanism

Fig. 3 Flapping mechanism of the AeroVironment Hummingbird [22]

motor using a crank-rocker mechanism with a gear which behvaes as the input crank to the wings as shown in Fig. 2. Each flapping wing has a four bar mechanism with separate outputs and share the input crank, hence, the wings can rotate independently. It is found that the maximum angle of attack at $45 degrees$ is aerodynamically optimal. The simple structure of the vehicle produces reasonable lift and drag coefficients, making passive pitch control feasible. The second mechanism is that of the AeroVironment hummingbird which weighs $19 grams$ with a payload including batteries, communication systems, motor and camera. The vehicle relies on motor driven crankshaft that is continuously rotating. The mechanism as shown in Fig. 3a, involves two strings that connect the crankshaft to the pulleys at the wing hinge flapping axis. Additionally, two other strings are used to connect the two pulleys. Therefore, the turning of the crankshaft driven by a motor results in the pulleys to oscillate which makes the wings flap as shown in Fig. 3b.

The AeroVironment hummingbird is designed using light weight and durable materials. The gears are made of PEEK, a strong plastic polymer, and the wing arms are carbon fiber with the wings made of flexible membrane. This makes the vehicle simple yet effective. Similar to the mechanism developed by Hu and Deng, the hummingbird uses passive pitch control by the flexibility of the wing which modifies the pitch as it flaps. The maximum angle of attack is controlled by mechanical stops, hence, the design is unsuitable for experimental setting like the Purdue mechanism. Another well-known mechanism is one developed by De Croon to control the DelFly which uses a crank mechanism that connects the motor to the wings [22]. Asymmetric motion of the wings causes a rotational movements. By modifying the drive train to be vertical to flight direction, the rotational effects can be neutralized. Lastly, the popular insect vehicle used in [20] to demonstrate the advantage of adaptive controller, called RoboBee, is designed to mimic the biological movement of insect wings by using a driving mechanism controlled by piezoelectric materials. Since it is a nano vehicle, it provides a small size envelope along with high speed performance at a low weight. This mechanism is called the Air force mechanism and the vehicle, shown in Fig. 4, demonstrates this technique. However, this driving mechanism also employs passive pitch control like the previous methodologies.

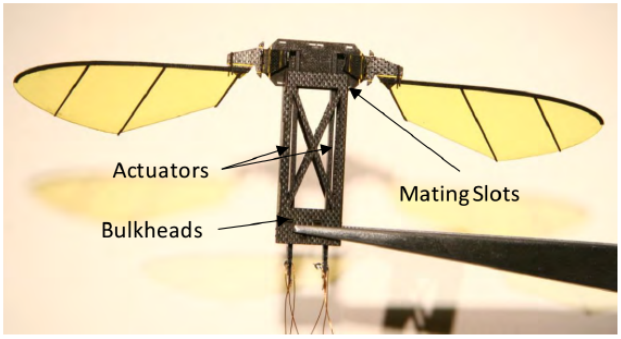

Fig. 4 Version of RoboBee that demonstrates the Air force mechanism

In [22], Balta et. al develop five prototypes inspired from the different mechanisms discussed and extrapolate the most efficient prototypes to create a viable design. The final design combines a gear driven system with a dual level design that imparts active pitch control. Figure 5 shows the mechanism of the prototype developed.

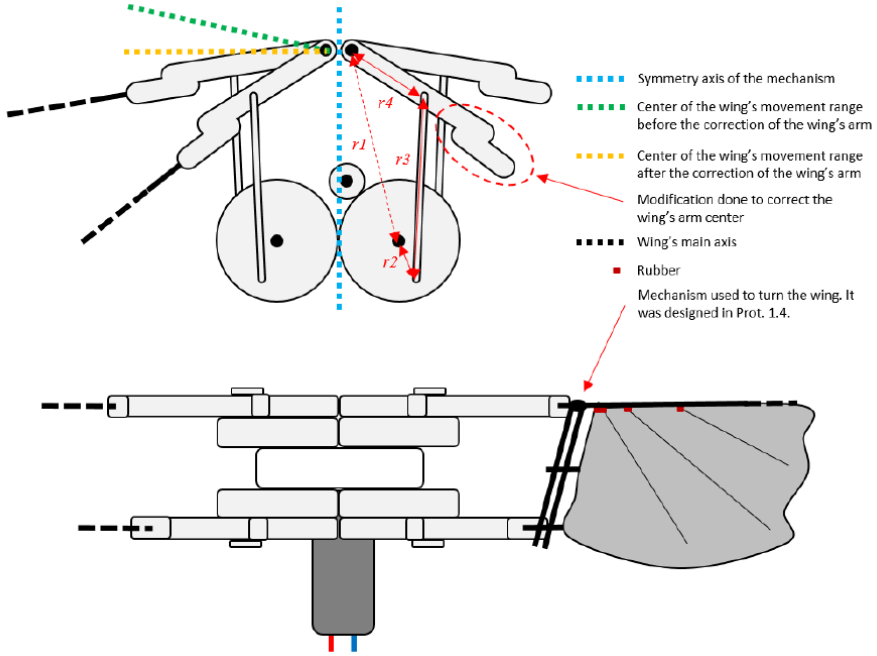

Fig. 5 Top and front view of the vehicle developed in [22]

The final prototype, shown in the above figure, uses the commercial mechanism of two crank rockers with gears as input cranks. This controls the swing of the wing, and the maximum wing pitch is controlled by mechanical stops added to an outer frame. The rate of change of wing pitch is controlled by including wing arms that run along guides on the frame. This setup allowed for an active pitching angle of $40 degrees$ during the testing of a previous prototype. Another mechanism included in the current prototype is the use of parallel crank rockers driven by a timing belt. This would allow for the model to yield theoretical ideal curves for wing swing and pitch. This mechanism was tested on a model built using laser cutters. The model provided desirable results, hence, it was added to the final prototype. A few other refinements were made the vehicle efficient, and are shown in Fig. 5. It was fabricated in a 3D printer using ABS plastic making the vehicle lighter than the other prototypes. The developed model successfully mimics the motion of hummingbird wings.

III. Aerodynamic Modeling

The flight dynamics of flapping flight has been of great interest for a while. It is a complex nonlinear, time varying multi body system. The research started out with the study of bird and insect flights. However, with the growing need of UAVs, the focus has shifted to designing flapping wing MAVs. The aerodynamics of FWMAVs utilise mechanisms such as LEV [9], and rotational lift and wake capture [10]. LEV is used for lift generation in delta wing aircrafts that undergo dynamic stall. However, for flapping flight, LEV has stable characteristics. Also, there is lift generated due to the rotation of the wing at each half stroke which is called rotational lift observed by Dickinson et. al in [10]. At the beginning of half strokes there is some additional lift caused by remaining wake from the previous half stroke which add to the total lift. A comprehensive table with aerodynamic models is compiled in [1] and is shown below in Table 1.

Properties	Dickinson et. al	Berman and Wang	UVLM
Computational Cost	✓	✓	–
LEV Contribution	✓	✓	×
Unsteadiness	×	×	✓
Rotational Lift	✓	✓	✓
Added Mass	✓	✓	✓
Wake Capture	×	×	✓
Viscous Friction	×	✓	×

Table 1 Comparison of aerodynamic models that are applicable to hovering MAVs [1].

As mentioned previously, Dickinson et. al [10] model incorporates LEV and has algebraic forms. Similarly, Breman and Wang [24] has algebraic forms, but takes viscousity into account in terms of viscous forces and dissipation. The unsteady vortex lattice method (UVLM) simulates vortex kinematics throughout the airfoil surface and its wake. Thus, the first two methods are cost effective and it appears as though there is no model that can account for the LEV contribution as well as the unsteadiness of hovering kinematics. The quasi-steady model developed by Dickinson et. al [10] is compact and provides algebraic expressions for coefficients of lift and drag as functions of angle of attack shown in Equations 12 and 13. Another compact quasi-steady model is developed by Wang et. al [25] where the drag and lift coefficients are calculated using experimentally obtained data.

$$C_L = 0.225 + 1.58 \sin(2.13\alpha - 7.20) \tag{12}$$

$$C_D = 1.92 - 1.55 \cos(2.04\alpha - 9.82) \tag{13}$$

However, these quasi-steady models do not account for the unsteady behavior of flapping flight and also do not translate well for different wing shapes, since the coefficients in both models are experimentally obtained in both models, it would change with varying aspect ratio. Therefore, a general formula for the lift coefficient is provided in [1] which would vary with aspect ratio as shown in Equation 14.

$$C_{L\alpha} = \frac{\pi AR}{1 + \sqrt{(\frac{\pi AR}{a_0})^2 + 1}} \tag{14}$$

where AR is the aspect ratio, i.e., $AR = \frac{R^2}{S}$. R is the wing radius and S is the wing planform area. In equation 14, a_0 is the lift curve slope of the two dimensional airfoil section

A. Approach

In [26], Taha et. al formulate the nonlinear, multi-body, time-varying mechanical equations taking into account the LEV and rotational effects for longitudnal flight. In the study of flapping flight aerodynamics two major assumptions are made: the wing inertial effects are considered negligible and the dynamics are averaged over a flapping cycle. Hence, in the model presented by Taha and Hassan in [1] the wing inertial effects are taken into consideration, making the model a multi-body formation. The four reference frames used to study the flight dynamics of a rigid wing FWMAV are shown in Fig. 6.

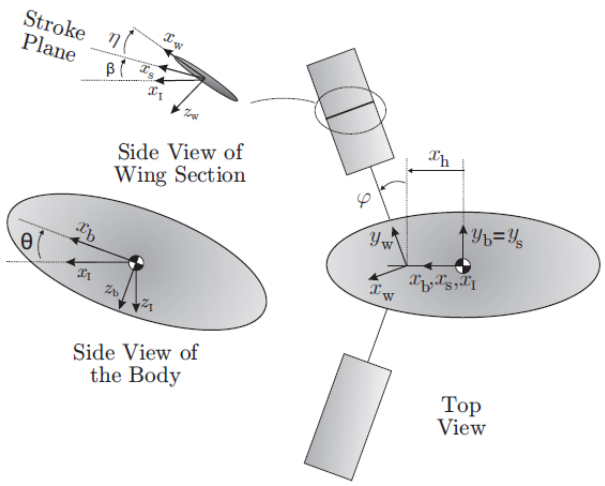

Fig. 6 FWMAV schematic diagram with four reference frames [26]

In Fig. 6, (x_I, y_I, z_I) is the inertial reference frame, (x_b, y_b, z_b) is the body-fixed reference frame, (x_s, y_s, z_s) is the stroke plane reference frame and (x_w, y_w, z_w) is the wing-fixed reference frame. The conventional Euler angle sequence of yaw-pitch-roll $(\psi - \theta - \phi)$ is shown, however, since longitudnal flight is considered, only θ is used for modeling. As shown in Fig.6, the wing is at an angle β from the horizontal plane, and it represents the stroke plane angle. The three Euler angles used to describe the wing motion are θ-ϕ-η. The out-of-stroke plane angle is denoted by θ and is called the plunging angle. In hover, insects have a horizontal stroke plane without an out of plane motion, i.e., $\theta = 0$. As emphasized by Doman et. al in [5], the Harvard Robofly's successful flight was attributed to minimal actuation. Hence, out-of-plane motion is not considered. The back and forth motion of the wing is denoted by ϕ and is called the flapping angle. The wing fixed frame is at an angle η from the stroke-plane, hence, η represents the pitching angle of the wing.

B. Implementation

The state space model used in this report is develeoped for unsteady aerodynamics of flapping flight by Taha and Hassan [26]. The state vector denoted by q has five states; $q = [x, z, \theta, \phi, \eta]$ where x and z are the displacements in the x and z direction, and θ, ϕ, η, are the three Euler angles. For FWMAVs in hover, the flapping kinematics is considered to be symmetric. The equations of motion are derived using the principle of virtual power which is then used to develop a rigorous and general aerodynamic model as shown in the following equations. This model accounts for "the nonlinear dependence of the non-autonomous aerodynamic loads on the aerodynamic state variables $(u, w, \dot{\theta})$" [26].

$$\begin{bmatrix} \frac{1}{m_w}X(x,t) \\ \frac{1}{m_w}Z(x,t) \\ \frac{1}{I_x}L(x,t) \\ \frac{1}{I_y}M(x,t) \\ \frac{1}{I_z}N(x,t) \end{bmatrix} = \begin{bmatrix} X_0(t) \\ Z_0(t) \\ L_0(t) \\ M_0(t) \\ N_0(t) \end{bmatrix} + \begin{bmatrix} X_u(t) & X_w(t) & X_q(t) \\ Z_u(t) & Z_w(t) & Z_q(t) \\ L_u(t) & L_w(t) & L_q(t) \\ M_u(t) & M_w(t) & M_q(t) \\ N_u(t) & N_w(t) & N_q(t) \end{bmatrix} \begin{pmatrix} u \\ w \\ \dot{\theta} \end{pmatrix} + \begin{pmatrix} X_{nl}(t) \\ Z_{nl}(t) \\ L_{nl}(t) \\ M_{nl}(t) \\ N_{nl}(t) \end{pmatrix} \tag{15}$$

$$X_0 = \rho\pi(kI_{11} - \frac{1}{4}I_{12})\sin\eta\dot{\eta}\dot{\phi} \tag{16}$$

$$Z_0 = -\frac{1}{2}\rho C_{L\alpha} I_{21}\sin\eta\dot{\phi}|\dot{\phi}| - \rho\pi(kI_{11} - \frac{1}{4}I_{12})\cos\eta\dot{\eta}\dot{\phi} \tag{17}$$

$$L_0 = -\frac{1}{2}\rho C_{L\alpha} I_{31}\sin\eta\dot{\phi}|\dot{\phi}| - \rho\pi(kI_{21} - \frac{1}{4}I_{22})\cos\eta\dot{\eta}\dot{\phi} \tag{18}$$

$$M_0 = \frac{3}{4}(-\frac{1}{2}\rho C_{L\alpha} I_{22}\sin\eta\dot{\phi}|\dot{\phi}| - \rho\pi(kI_{12} - \frac{1}{4}I_{13})\cos\eta\dot{\eta}\dot{\phi}) - kZ_0 \tag{19}$$

$$N_0 = -\rho\pi(kI_{21} - \frac{1}{4}I_{22})\sin\eta\dot{\eta}\dot{\phi} \tag{20}$$

$$X_u = \rho\pi(kI_{01} - \frac{1}{4}I_{02})(\cos\beta\sin\eta\cos\phi + \sin\beta\cos\eta)\dot{\eta} \tag{21}$$

$$X_w = -\rho\pi(kI_{01} - \frac{1}{4}I_{02})(\sin\beta\sin\eta\cos\phi - \cos\beta\cos\eta)\dot{\eta} \tag{22}$$

$$\begin{aligned} X_q =& \rho\pi(kI_{11} - \frac{1}{4}I_{12})\sin\eta\cos\phi\dot{\phi} - \rho\pi(x_h(kI_{01} - \frac{1}{4}I_{02})(\cos\eta\cos(\beta-\theta) - \sin\eta\cos\phi\sin(\beta-\theta)) \\ &+ \cos\eta\sin\phi(kI_{11} - \frac{1}{4}I_{12}))\dot{\eta} \end{aligned} \tag{23}$$

$$\begin{aligned} X_{nl} =& \rho\pi\cos\phi\dot{\theta}(kI_{01} - \frac{1}{4}I_{02})(u(\cos\beta\sin\eta\cos\phi + \sin\beta\cos\eta) + w(\cos\beta\cos\eta - \sin\beta\sin\eta\cos\phi)) \\ &- \rho\pi(x_h\cos\phi(kI_{01} - \frac{1}{4}I_{02})(\cos\eta\cos(\beta-\theta) - \sin\eta\cos\phi\sin(\beta-\theta)) + \cos\eta\sin\phi(kI_{11} - \frac{1}{4}I_{12}))\dot{\theta}^2 \end{aligned} \tag{24}$$

$$Z_u = -\frac{1}{2}\rho C_{L\alpha}I_{11}(2\cos\beta\sin\eta\cos\phi + \sin\beta\cos\eta)|\dot{\phi}| - \rho\pi(kI_{01} - \frac{1}{4}I_{02})(\cos\beta\cos\eta\cos\phi - \sin\beta\sin\eta)\dot{\eta} \tag{25}$$

$$Z_w = \rho\pi(kI_{01} - \frac{1}{4}I_{02})(\sin\beta\cos\eta\cos\phi + \cos\beta\sin\eta)\dot{\eta} - \frac{1}{2}\rho C_{L\alpha}I_{11}(\cos\beta\cos\eta - 2\sin\beta\sin\eta\sin\eta\cos\phi)\dot{\phi} \tag{26}$$

$$\begin{aligned} Z_q =& \frac{1}{2}\rho C_{L\alpha}I_{21}\cos\eta\sin\phi|\dot{\phi}| \\ &+ \rho C_{L\alpha}I_{11}|\dot{\phi}|(x_h\sin\beta\sin\eta\cos\theta\cos\phi + \frac{1}{2}\cos\beta(2x_h\sin\eta\sin\theta\cos\phi + x_h\cos\eta\cos\theta) \\ &+ \frac{1}{2}x_h\sin\beta\cos\eta\sin\theta) + \rho\pi x_h\cos\eta\cos\phi\sin(\beta-\theta)(\frac{1}{4}I_{02} - kI_{01})\dot{\eta} \\ &+ \rho\pi x_h\sin\eta\cos(\beta-\theta)(\frac{1}{4}I_{02} - kI_{01})\dot{\eta} - \rho\pi\sin\eta\sin\phi(kI_{11} - \frac{1}{4}I_{12})\dot{\eta} - \rho\pi\cos\eta\cos\phi(kI_{11} - \frac{1}{4}I_{12})\dot{\phi} \end{aligned} \tag{27}$$

$$\begin{aligned} Z_{nl} =& -\rho\pi\cos\phi\dot{\theta}(kI_{01} - \frac{1}{4}I_{02})(u(\cos\beta\cos\eta\cos\phi - \sin\beta\sin\eta) + w(\sin\beta\cos\eta\cos\phi + \cos\beta\sin\eta)) \\ &+ \dot{\theta}^2(2\pi\rho x_h\cos\phi(\frac{1}{4}I_{02} - kI_{01})(\cos\eta\cos\phi\sin(\beta-\theta) + \sin\eta\cos(\beta-\theta)) \\ &- 2\pi\rho\sin\eta\sin\phi\cos\phi(kI_{11} - \frac{1}{4}I_{12})) \end{aligned} \tag{28}$$

$$L_u = -\frac{1}{2}\rho C_{L\alpha} I_{21}(2\cos\beta\sin\eta\cos\phi + \sin\beta\cos\eta)|\dot{\phi}| - \rho\pi(kI_{11} - \frac{1}{4}I_{12})(\cos\beta\cos\eta\cos\phi - \sin\beta\sin\eta)\dot{\eta} \tag{29}$$

$$L_w = \rho\pi(kI_{11} - \frac{1}{4}I_{12})(\sin\beta\cos\eta\cos\phi + \cos\beta\sin\eta)\dot{\eta} - \frac{1}{2}\rho C_{L\alpha} I_{21}(\cos\beta\cos\eta - 2\sin\beta\sin\eta\cos\phi)|\dot{\phi}| \tag{30}$$

$$\begin{aligned} L_q =& \frac{1}{2}\rho C_{L\alpha} I_{31}\cos\eta\sin\phi|\dot{\phi}| + \rho C_{L\alpha} I_{21}|\dot{\phi}|(x_h\sin\beta\sin\eta\cos\theta\cos\phi \\ &+ \frac{1}{2}\cos\beta(2x_h\sin\eta\sin\theta\cos\phi + x_h\cos\eta\cos\theta) + \frac{1}{2}x_h\sin\beta\cos\eta\sin\theta) \\ &+ \rho\pi x_h(\frac{1}{4}I_{12} - kI_{11})\dot{\eta}(\cos\eta\cos\phi\sin(\beta-\theta) + \sin\eta\cos(\beta-\theta)) \\ &- \rho\pi(kI_2 1 - \frac{1}{4}I_{22})(\sin\eta\sin\phi\dot{\eta} - \cos\eta\cos\phi\dot{\phi}) \end{aligned} \tag{31}$$

$$\begin{aligned} L_{nl} =& -\rho\pi\cos\phi(kI_{11} - \frac{1}{4}I_{12})(\cos\beta\cos\eta\cos\phi - \sin\beta\sin\eta)\dot{\theta}u \\ &+ \rho\pi\cos\phi(kI_{11} - \frac{1}{4}I_{12})(\sin\beta\cos\eta\cos\phi + \cos\beta\sin\eta)|\dot{\theta}|w \\ &+ |\dot{\theta}|^2(2\rho - \pi x_h\cos\phi(\frac{1}{4}I_{12} - kI_{11})(\cos\eta\cos\phi\sin(\beta-\theta) + \sin\eta\cos(\beta-\theta)) \\ &- 2\rho\pi\sin\eta\sin\phi\cos\phi(kI_{21} - \frac{1}{4}I_{22})) \end{aligned} \tag{32}$$

$$\begin{aligned} M_u =& \frac{3}{4}(-\frac{1}{2}\rho C_{L\alpha} I_{12}(2\cos\beta\cos\eta\cos\phi + \sin\beta\sin\eta)\dot{\eta}) \\ &- kZ_u \end{aligned} \tag{33}$$

$$\begin{aligned} M_w =& \frac{3}{4}(\rho\pi(kI_{02} - \frac{1}{4}I_{03})(\sin\beta\cos\eta\cos\phi + \cos\beta\sin\eta)\dot{\eta} - \frac{1}{2}\rho C_{L\alpha} I_{12}(\cos\beta\cos\eta - 2\sin\beta\sin\eta\cos\phi)|\dot{\phi}|) \\ &- kZ_w \end{aligned} \tag{34}$$

$$\begin{aligned} M_q =& \frac{3}{4}(\frac{1}{2}\rho C_{L\alpha} I_{22}\cos\eta\sin\phi|\dot{\phi}| + \rho C_{L\alpha} I_{12}|\dot{\phi}|[x_h\sin\beta\sin\eta\cos\theta\cos\phi \\ &+ \frac{1}{2}\cos\beta(2x_h\sin\eta\sin\theta\cos\phi + x_h\cos\eta\cos\theta) + \frac{1}{2}x_h\sin\beta\cos\eta\sin\theta] \\ &+ \rho\pi x_h\cos\eta\cos\phi\sin(\beta-\theta)(\frac{1}{4}I_{03} - kI_{02})\dot{\eta} + \rho\pi x_h\sin\eta\cos(\beta-\theta)(\frac{1}{4}I_{03} - kI_{02})|\dot{\eta}| \\ &- \rho\pi\sin\eta\sin\phi(kI_{12} - \frac{1}{4}I_{13})\dot{\eta} - \rho\pi\cos\eta\cos\phi(kI_{12} - \frac{1}{4}I_{13})\dot{\phi}) - kZ_q \end{aligned} \tag{35}$$

$$\begin{aligned} M_{nl} =& \frac{3}{4}(-\rho\pi(kI_{02} - \frac{1}{4}I_{03})\cos\phi\dot{\theta}[u(\cos\beta\cos\eta\cos\phi - \sin\beta\sin\eta) - w(\sin\beta\cos\eta\cos\phi + \cos\beta\sin\eta)] \\ &+ \dot{\theta}^2[2\rho\pi x_h(\frac{1}{4}I_{03} - kI_{02})\cos\phi(\cos\eta\cos\phi\sin(\beta-\theta) + \sin\eta\cos(\beta-\theta)) \\ &- 2\rho\pi(kI_{12} - \frac{1}{4}I_{13})\sin\eta\sin\phi\cos\phi] - kZ_{nl} \end{aligned} \tag{36}$$

$$N_u = -\rho\pi(kI_{11} - \frac{1}{4}I_{12})(\cos\beta\sin\eta\cos\phi + \sin\beta\cos\eta)|\dot{\eta}| \tag{37}$$

$$N_w = \rho\pi(kI_{11} - \frac{1}{4}I_{12})(\sin\beta\sin\eta\cos\phi - \cos\beta\cos\eta)\dot{\eta} \tag{38}$$

$$\begin{aligned} N_q =& \rho\pi(x_h(kI_{11} - \frac{1}{4}I_{12})(\cos\eta\cos(\beta-\theta) - \sin\eta\cos\phi\sin(\beta-\theta)) + \cos\eta\sin\phi(kI_{21} - \frac{1}{4}I_{22}))\dot{\eta} \\ & - \rho\pi(kI_{21} - \frac{1}{4}I_{22})\sin\eta\cos\phi\dot{\phi} \end{aligned} \tag{39}$$

$$\begin{aligned} N_{nl} =& -\rho\pi(kI_{11} - \frac{1}{4}I_{12})\cos\phi\dot{\theta}(u(\cos\beta\sin\eta\cos\phi + \sin\beta\cos\eta) + w(\cos\beta\cos\eta - \sin\beta\sin\eta\cos\phi)) \\ & + \rho\pi|\dot{\theta}|^2(x_h\cos\phi(kI_{11} - \frac{1}{4}I_{12})(\cos\eta\cos(\beta-\theta) - \sin\eta\cos\phi\sin(\beta-\theta)) + \cos\eta\sin\phi(kI_{21} - \frac{1}{4}I_{22})) \end{aligned} \tag{40}$$

In the above Eq. 15, X and Z are the aerodynamic loads and L, M, N are the moments, m_w is the mass of the wing, I_x, I_y and I_z are the moment of inertia about x,y and z axis, respectively. The constant k is calculated as $k = c_r(1 - x_{or})$ where c_r is the root chord, x_{or} is the normalized distance of the hinge point from the origin and x_h is the position of the hinge point with respect to the center of mass. Also, I_{mn} is calculated as $I_{mn} = 2\int_0^R r^m c^n(r)dr$ where R is the wing radius and $c(r)$ is the spanwise chord distribtution. Additionally, ρ is the air density and $C_{L\alpha}$ is the three dimensional lift curve slope calculated using equation14. These equations are plugged into a Simulink to block diagram to get the aerodyanmic loads and moments as shown in Fig. 7.

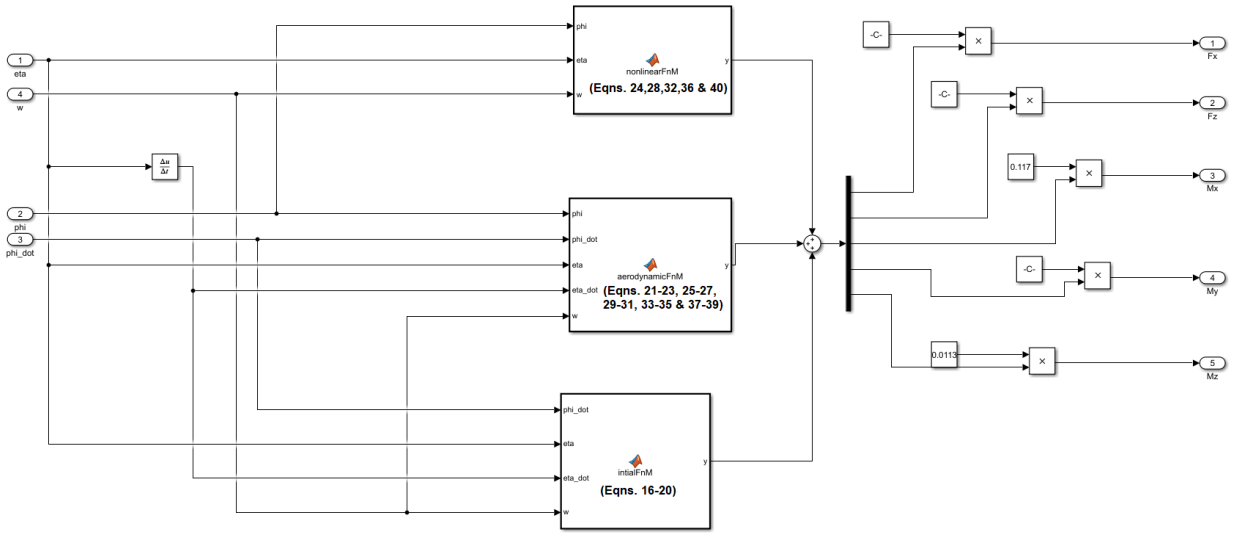

Fig. 7 Aerodynamic block diagram on Simulink.

In the above block diagram, Eq. 15 is represented in the form of Matlab function blocks. The block *initialFnM* using Eqs. 16-20 calculates the initial loads and moments denoted by (X_0, Z_0, L_0, M_0, N_0), the block *aerodynamicFnM* using Eqs. 21-23, 25-27, 29-31,33-35 and 37-39 calculates the forces and moments with respect to the states and the block *nonlinearFnM* using Eqns. 24, 28, 32, 36 and 40 calculates the nonlinear forces and moments. The aerodynamic block receives the Euler angles $\eta - \phi - \theta$ as inputs. The forces and moments from the blocks are then multiplied by the appropriate constants to get the total forces and moments matrix.

IV. Control Design

The aerodynamic-dynamic interaction can be created by relating the forces and moments from the aerodynamic model to the averaged dynamics of flapping flight. The aerodynamic load experienced by a vehicle is controlled by the velocity vector of the wing. However, in the case of hovering kinematics, the speed of flapping is the major factor. As mentioned in Section 1.D, cycle-averaging of the flight dynamics produces the least erroneous results. In [1], Taha and Hassan take into consideration the aerodynamic loads relative to the body motion in a "full nonlinear sense" which yields a tightly linked aerodynamic and dynamic interaction. A schematic representation of the aerodynamic-dynamic interaction is shown in Fig. 8.

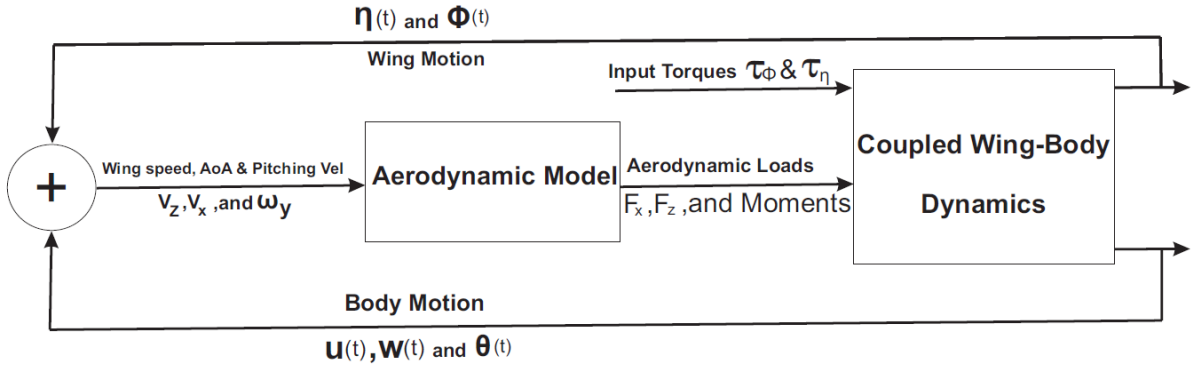

Fig. 8 A schematic drawing of the aerodynamic-dynamic interaction from [1].

The flight dynamic model credited to Taha and Hassan in [27] is used to simulate the dynamics. The original model, with five degrees of freedom, is reduced to three: two for the body, z which is the body displacement in vertical direction and θ which is the body pitching angle, and one for the wing, ϕ which is the flapping angle. The pitching angle of the wing (η) is assumed to vary based on the rate of change of flapping angle as shown in equation 41.

$$\eta(t) = \begin{Bmatrix} \alpha_m, & \dot{\phi} > 0 \\ \pi - \alpha_m, & \dot{\phi} < 0 \end{Bmatrix} \tag{41}$$

where α_m is the mean angle of attack of the flapping wing. Hence the reduced order model in[27] is shown in Eq. 42.

$$M(q; sign(\dot{\phi}))\ddot{q} + f_c(q, \dot{q}) = f_{aero} + g\tau_\phi \tag{42}$$

$$M = \begin{bmatrix} m_v & M_{12} & M_{13} \\ M_{21} & M_{22} & M_{23} \\ 0 & 0 & I_{yb} \end{bmatrix} \tag{43}$$

$$\begin{aligned}
M_{12} &= -r_{cg}\cos\phi\sin\theta - \bar{c}\hat{d}\cos\alpha_m sign(\dot{\phi})\sin\phi\sin\theta \\
M_{13} &= \bar{c}\hat{d}\cos\alpha_m\sin\theta - r_{cg}\cos\theta\sin\phi \\
M_{21} &= -m_w r_{cg}\cos\phi\sin\theta - \bar{c}\hat{d}m_w\cos\alpha_m sign(\dot{\phi})sign(\phi)\sin\theta \\
M_{22} &= -\frac{1}{2}I_{xw}\cos{\alpha_m}^2 - \frac{1}{2}I_{zw}\sin{\alpha_m}^2 + \frac{I_F}{2} + \frac{I_{xw}+I_{zw}}{2} \\
M_{23} &= \frac{1}{2}(I_{zw} - I_{xw})sign(\dot{\phi})\sin(2\alpha_m)\sin phi
\end{aligned}$$

$$f_c = \begin{bmatrix} -\dot{\theta}^2(\overline{c}\hat{d}\sin\alpha_m\cos\theta + \overline{c}\hat{d}\cos\alpha_m\sin\theta sign(\dot{\phi})\cos\phi - r_{cg}\sin\theta\sin\phi) \\ -2\dot{\theta}\dot{\phi}(\overline{c}\hat{d}\cos\alpha_m\cos\theta sign((\dot{\phi})\sin\phi + r_{cg}\cos\theta\cos\phi) \\ +\dot{\phi}^2(r_{cg}\sin\theta\sin\phi - \overline{c}\hat{d}\cos\alpha_m\sin\theta sign(\dot{\phi})\cos\phi) - gm_v \\ \\ -\dot{\theta}w(\overline{c}\hat{d}m_w\cos\alpha_m\cos\theta sign(\dot{\phi}) + m_w r_{cg}\cos\theta\cos\phi) \\ +w\dot{\phi}(m_w r_{cg}\sin\theta\sin\phi - \overline{c}\hat{d}m_w\cos\alpha_m\sin\theta sign(\dot{\phi})\cos\phi) \\ +\dot{\theta}^2(\frac{1}{2}\cos{\alpha_m}^2(I_{zw} - I_{xw})\sin\phi\cos\phi + \frac{1}{2}\sin{\alpha_m}^2(I_{xw} - I_{zw})\sin\phi\cos\phi \\ +\frac{1}{2}(-I_{xw} - I_{zw})\sin\phi\cos\phi + \frac{1}{2}I_{yw}\sin 2\phi) \\ \\ 0 \end{bmatrix} \tag{44}$$

$$f_{aero} = \begin{bmatrix} -F_x(\sin\alpha_m\cos\theta + \cos\alpha_m\sin\theta sign(\dot{\phi})\cos\phi) - F_z(\sin\alpha_m\sin\theta\cos\phi - \cos\alpha_m\cos\theta sign(\dot{\phi})) \\ \\ \sin\alpha_m M_x - \cos\alpha_m M_z sign(\dot{\phi}) \\ \\ -\cos\alpha_m M_x sign(\dot{\phi}) + M_y\cos\phi - \sin\alpha_m M_z\sin\phi \end{bmatrix} \tag{45}$$

where M is the inertia matrix and can be calculated using Eq.43, f_c contains force terms related to coriolis and centripetal effects, f_{aero} represents the aerodynamic loads that was calculated in the previous section and τ_ϕ is the input torque. The dynamics equation from 46 is rewritten to make it programmable for geometric control analysis as follows

$$\dot{x} = Z(x) + Y(x)\tau_\phi(t) \tag{46}$$

where

$$Z(x) = \begin{bmatrix} \dot{q} \\ M^{-1}(f_{aero} - f_c) \end{bmatrix} \tag{47}$$

and

$$Y(x) = \begin{bmatrix} 0 \\ M^{-1}g \end{bmatrix} \tag{48}$$

The input torque applied to the wing is a cosine wave and is connected to the dynamic block using a sine wave block with a phase of 90°. Due to the reduction of the order of the model, there is no input torque to control η. Therefore, η is calculated by creating a time delay from the ϕ signal and adding a gain block to operate the vehicle as per requirement. The implementation of the flight dynamics in Simulink is shown in Fig. 9 below.

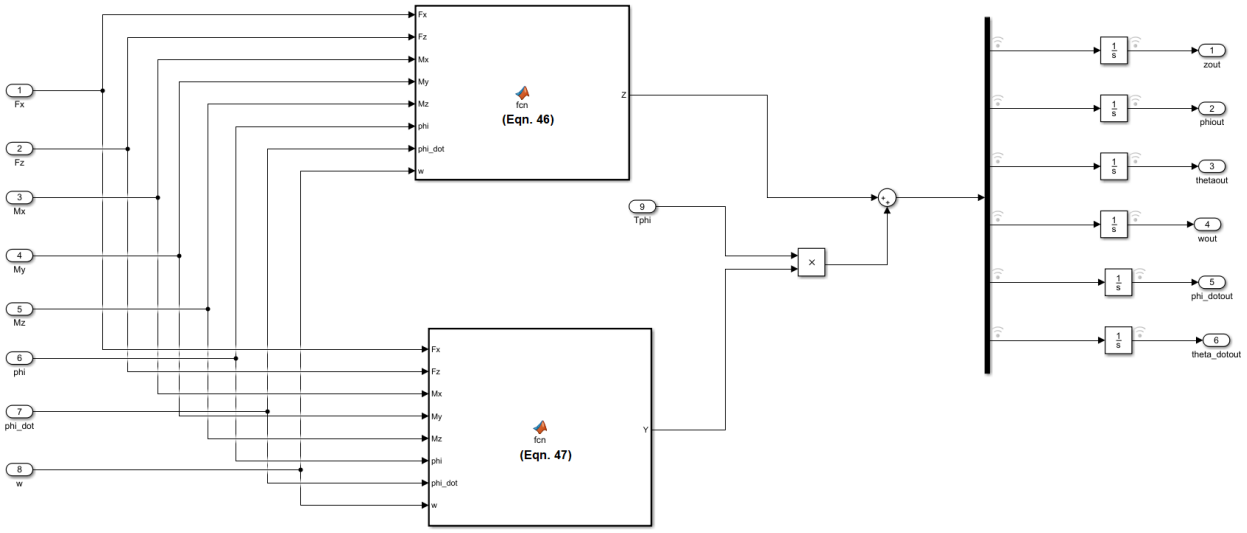

Fig. 9 Flight dynamic block diagram on Simulink.

To simulate the dynamics in Simulink, two Matlab function blocks were set up. One function block calculates $Z(x)$ given by Eq. 47 and the other calculates $Y(x)$ given by Eq. 48 which are used in Eq. 46. This gives the first order derivative of the states, $\dot{x}$. This signal is passed through an integrator block with initial condition set at 0 for all states to calculate the instataneous states.

A. Averaging tools

Averaging can be used for the conversion of non-autonomous system to autonomous system. In [27], the averaging theorem is explored in an attempt to make the current model autonomous. The averaging theorem can be applied to any smooth vector field. The state vector $X(x,t)$ of flight dynamics must be averaged, however, it is not smooth in all its states. Instead the generalized averaging theory, introduced by Sarychev in[28], performs a complete averaging using Lie brackets between two vector fields. Additionally, variation of constants formula (VOC) can be applied to systems subjected to high amplitude period forcing, to make the system receptive to direct averaging. Using the VOC yields a pullback vector that can be averaged to get the averaged dynamics of the original system.

Equation 46 describes the flight dynamics of a non-autonomous FWMAV. However, by applying direct averaging theorem, the system produces trivial results causing no effect of flapping on dynamics. Therefore, VOC is applied to the system 46 to get the pullback vector, as shown in Eq. 49.

$$F(x,t) = Z(x) + [Y,Z]\int_0^t \tau_\phi(s_1)ds_1 + [Y,[Y,Z]]\int_0^t\int_0^{s_1} \tau_\phi(s_2)\tau_\phi(s_1)ds_2ds_1 \tag{49}$$

where $F(x,t)$ represents the pullback vector, Z and Y are the vectors from the original system 46 and τ_ϕ is the input torque.

V. Results

The simulation is set up as shown in Fig. 10. The aerodynamic block shown in the figure below calculates the forces and moments using equations listed in section III.B and the dynamic block computes the vertical displacement and velocity, and flapping angle and rate according to section IV. The only control input is the torque controlling the flapping angle, τ_ϕ.

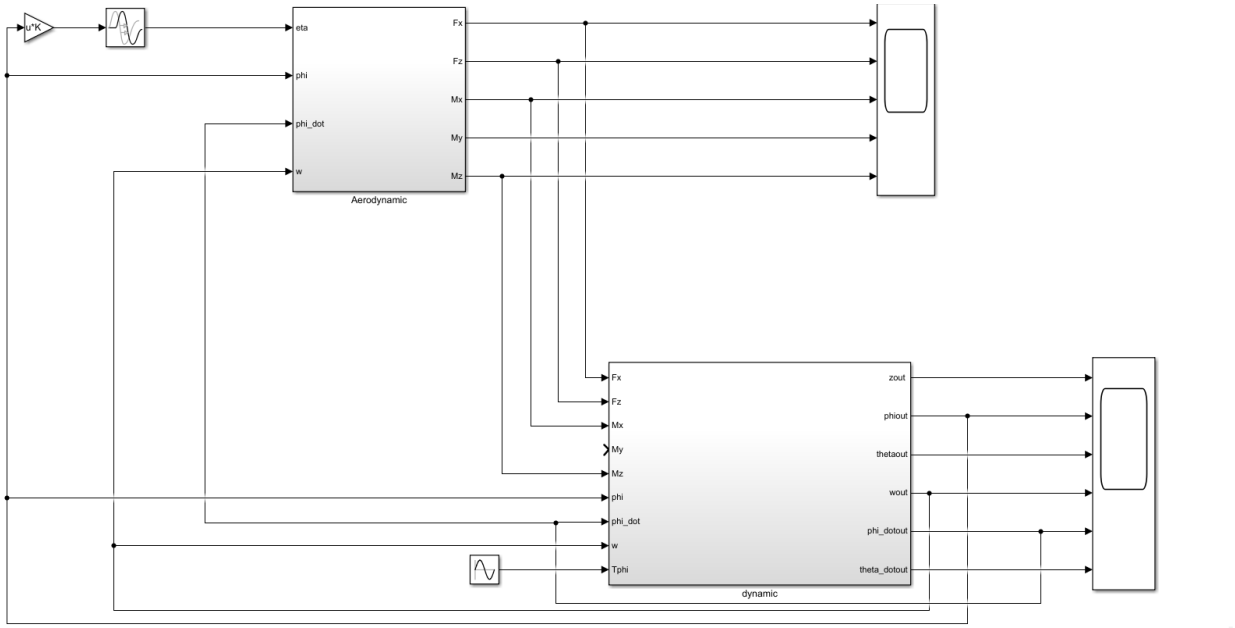

Fig. 10 Simulink block diagram of flapping wing vehicle.

Since there is no active pitch control, the pitching moment M_y computed in the aerodynamic block is not used to calculate the states in the dynamic block. To run the model, the morphological parameters of the Hawkmoth are used as described in [29], in which the full kinematics in the longitudnal direction of major insects is detailed.

$$R = 51.9mm \qquad S = 947.8mm^2 \qquad \overline{c} = 18.33mm,$$
$$\hat{r_1} = 0.44 \qquad \hat{r_2} = 0.525,$$
$$m_b = 1.648g \qquad I_{yb} = 2.080 * 10^{-2} g.mm^2$$

The simulation time is set to 10 seconds and the control input is manipulated to acheive different flight conditions. Figures 11, 12 and 13 show the states: displacement, flapping angle, vertical velocity and flapping rate in ascend, descend and hover. The units for vertical displacement and velocity are mm and mm/sec, respectively. Similarly, the units for flapping angle and rate are rad and rad/sec. As shown for the case of negative vertical displacement, i.e., climbing flight condition in Fig. 11, there is an initial downward movement, represented by z, which converts to ascending flight as the vehicle continues flapping shown by negative displacement since z points downwards. Hence, the vertical displacement is $\pm 2m$ with the final position of the vehicle at $2m$. The vertical velocity, denoted by w, has a positive value initially which validates the initial positive displacement in the downward direction. The flapping angle and rate, which is controlled by τ_ϕ, are also shown in Fig. 11 denoted by ϕ and $\dot{\phi}$. The flapping rate is a sinusoidal wave with a constant amplitude. However, due to noise in the flapping rate signal, the integration yields a rising flapping angle signal with small difference of $0.2rad$ between the initial and final peaks.

On the other hand, Fig. 12 shows the gradual descent of the vehicle. The vertical velocity, represented by w in the third signal, experiences a positive change, peaks and settles down at a steady state value of $0mm/sec$. This is reflected in vertical displacement, represented by z in the first signal, in which the displacement reaches a steady state value of $8m$ in the downward direction. The flapping angle and rate, represented by the second and fourth signal respectively, yield similar results to ascending flight conditions. The flapping rate signal is a sinusoidal wave with a constant amplitude and some noise, whereas the flapping angle is a rising sinusoidal wave as a result of integration of the noise; due to the difference in the ranges of the amplitude of the flapping rate signal compared to flapping angle signal, any small disturbance in$\dot{\phi}$ appears large in ϕ.

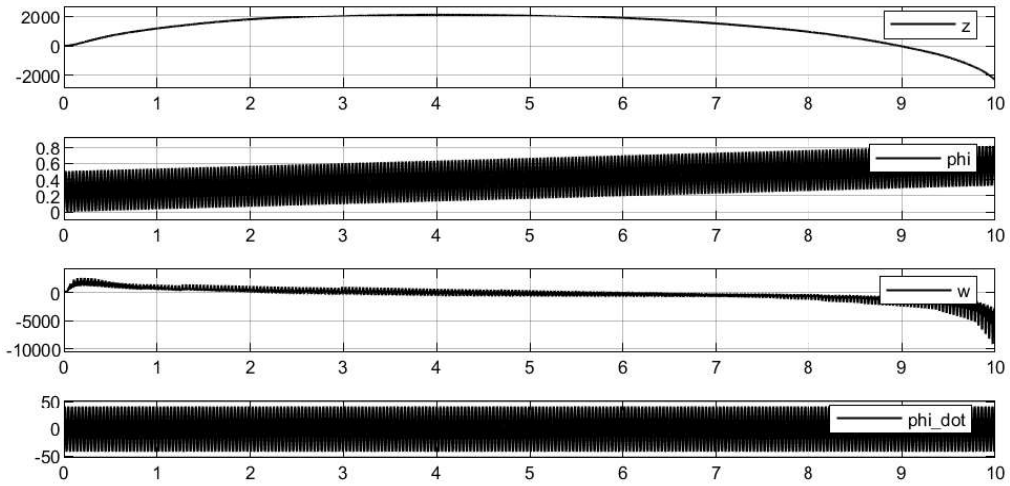

Fig. 11 Signals generated for the flight condition of ascend.

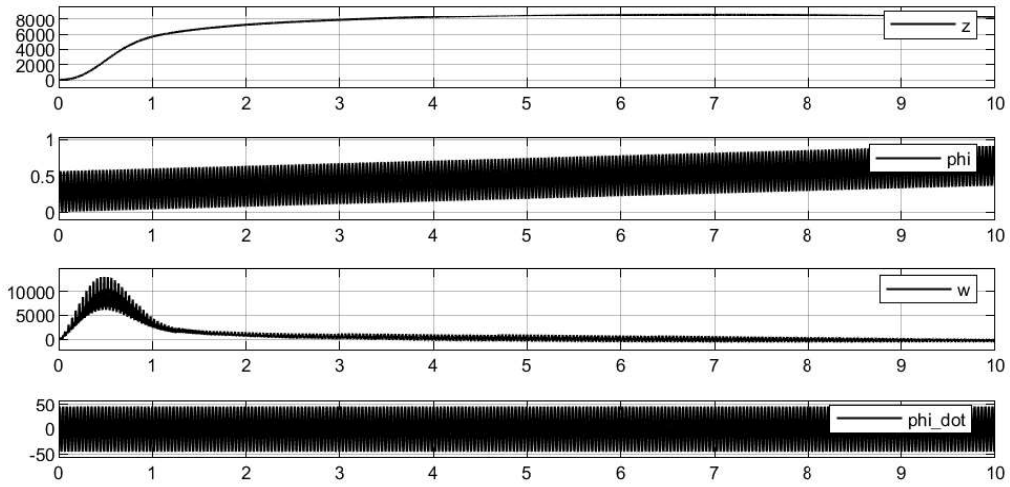

Fig. 12 Signals generated for the flight condition of descend.

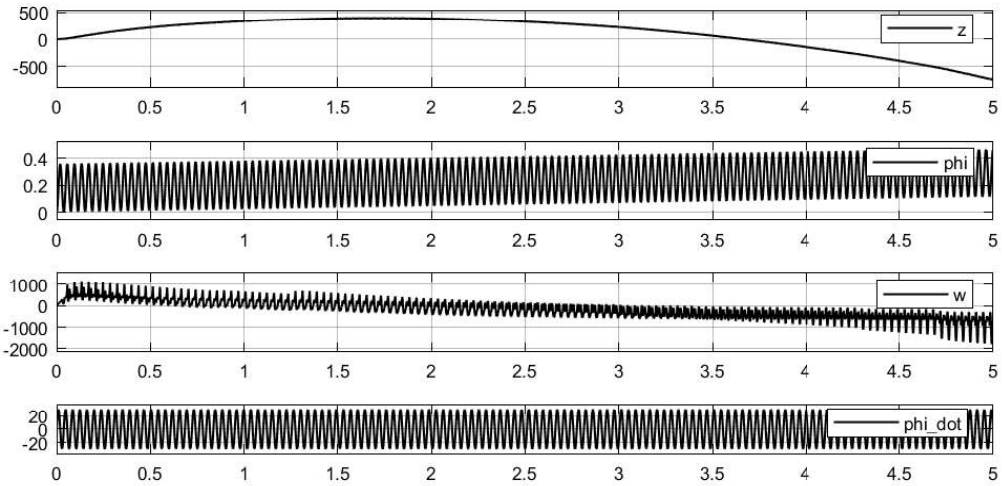

Fig. 13 Signals generated for the flight condition of hover.

The third flight condition this vehicle obtained is hover as shown in in Fig. 13. The simulation time is set to $5sec$ as opposed to $10sec$ in the case of ascent and descent. The frequency of the input torque τ_ϕ is $165.25rad/sec$ and the relation presented in Eq. 50 between the flapping and torque amplitude is used to approximate the input torque.

$$\phi = \frac{U}{\omega^2 I_x \sin {\alpha_m}^2} \tag{50}$$

In eq. 50, ϕ is the flapping angle, ω is the angular freqeuncy calculated from the natural frequency of a Hawkmoth, i.e. $26.3Hz$ or $165.25rad/sec$, I_x is the moment of inertia about the x axis of the wing and U is the amplitude of the input torque, which is represented as a sinusoidal function as shown in eq. 51.

$$\tau_\phi = U \cos \omega t \tag{51}$$

In fig. 13, the vertical displacement is $\pm.5m$ yielding a hovering motion with an initial downward movement and then an equal upward movement. The flapping angle and rate yield results similar to the ascent and descent case. To obtain these conditions the parameters for the input torque along with the flapping and wing pitch angle relation are modified as shown in Table 2.

Flight Condition	Amplitude of input torque	Displacement (in mm)	Flapping angle(in rad)	Gain
Ascend	5953200	±2000	±0.45	9
Descend	6571200	−8000	±0.55	7
Hover	4220050	±500	±0.39	15

Table 2 Parameters for different flight conditions at frequency 165 rad/sec (or 26Hz).

VI. Conclusion

With the growing interest in FWMAVs, there has been a focus set on understanding the dynamics of insect flight. Research shows that insect flight can not be explained using conventional aircraft flight dynamic models. This report summarizes significant work done in understanding the flight of flapping wing vehicles. A comprehensive review of the current aerodynamic models, flight dynamics, control approaches and actuation mechanisms has beeen performed. Based on the literature review, there is not any aerodynamic model that account for the unsteadiness as well as consider hovering mechanisms of insects simultaneously.

Taha in [1] developed "an unsteady aerodynamic model whose asymptotic steady behavior is dictated by the empirical models that capture the quasi-steady effects of the leading edge vortex." Along with this, an analytical flight

dynamic model that captures the high lift mechanisms of insect flight is included. This nonlinear flight dynamic model, produces erroneous results from direct averaging. Hence, it goes through cycle averaging to yield steady flight. This is established by using VOC formula to produce a pullback vector which is then averaged. However for the scope of this project the nonlinear flight dynamic is implemented ignoring the moment about the y axis since there is no active pitch control. The actuation mechanism used to drive the vehicle is through input torques that control the flapping of the wing. The model does not include active pitch control, hence, the moment about y-axis is considered zero rendering the body pitch angle and body pitch rate to be non-contributing states. To demonstrate the validity of the model, properties associated with Hawkmoth are used to run the simulation. Using the aerodynamic model presented in [26] combined with the flight dynamic model from [27] presented by Taha et. al, the results produced show that the presented model functions by controlling the input torque and yields desirable outputs for different flight conditions. By changing the amplitude of the actuating torque, which alters the flapping angle, and also changing the wing pitch angle, the model is able to ascend, descend and hover.

Including active pitch control of the flapping wings requires complex computation which can result in expensive computation cost. However, to produce accurate results such actuation mechanisms need to be modeled. Also, with a more complex system a robust controller with adaptive control can be considered incorporation with simple analytical aerodynamic model. Since, hover is a highly demanded feature in insect flight, more research needs to be done in the transition phase from forward flight to hover. Additionally, control laws need to be developed to conduct this transition effectively.

References

[1] Taha, H., "Mechanics of Flapping Flight: Analytical Formulations of Unsteady, Aerodynamics, Kinematic Optimization, Flight Dynamics, and Control", Ph.D. Dissertation, Virginia Polytechnic Institute and State University, Blacksburg, Virginia, 2013.

[2] Wang, Q., Goosen, H., and Keulen, F., "Optimal Hovering Kinematics with respect to Various Flapping-Wing Shapes", *International Micro Air Vehicle Conference and Flight Competition*, IMAV2013, CSAA, 2013, pp. 17-20.

[3] Abas, M.F.B, Rafie, A.S.B., Yusoff, H.B., and Ahmad, K.A.B., "Flapping wing micro-aerial vehicle: kinematics, membranes, and flapping mechanisms of ornithopter and insect flight", *Chinese Journal of Aeronautics*, Vol. 29, No. 5, 2016, pp. 1159,1177.

[4] Schenato, L., Campolo, D., and Sastry, S., "Controllability issues in flapping flight for biomimetic micro aerial vehicles (MAVs)", *IEEE Conference on Decision and Control*, IEEE, 2003.

[5] Doman, D.B., Oppenheimer, M.W., and Sigthorsson, D.O., "Wingbeat shape Modulation for Flapping-Wing Micro-Air Vehicle Control During Hover", *Journal of Guidance, Control and Dynamics*, Vol. 33, No. 3, 2010, pp. 724,739.

[6] Hopper, S.L., "Central Pattern Generators", *eLS*, 2001.

[7] Chung. S., and Dorothy, M., "Neurobiologically Inspired Control of Engineering Flapping Flight", *Journal of Guidance, Control, and Dynamics*, Vol. 33, No. 2, 2010, pp. 440,453.

[8] Holst, E.v., and Kuchemann, D., "Biologische und aerodynamische Probleme des Tierfluges", *Die Naturwissenschaften*, pp 348-376.

[9] Ellington, C.P., Coen, B., Willmott, A.P., and Thomas, A.L.R., "Leading-Edge Vortices in Insect Flight", *Nature: International Journal of Science*, Vol. 384, 1996, pp. 626,630.

[10] Dickinson, M.H., Lehmann, F., and Sane, S.P., "Wing Rotation and the Aerodynamic Basis of Insect Flight", *Science*, Vol. 284, No. 5422, 1999, pp. 1954,1960.

[11] Khan, Z.A., and Agrawal, S.K., "Force and Moment Characterization of Flapping Wings for Micro Aerial Vehicle Application", *American Control Conference*, AACC, 2005.

[12] Pesavento, U., and Wang, Z.J., "Navier stokes solutions, model of fluid forces and center of mass elevation", *Phys. Rev. Lett.,* Vol. 93, 2004.

[13] Orlowski, C.T., and Girard, A.R., "Modeling and Simulation of Nonlinear Dynamics of Flapping WIng Micro Air Vehicles", *AIAA Journal*, Vol. 49, No. 5, 2011, pp. 969,982.

[14] Nayfeh, A.H., and Mook, D.T., "Energy Transfers from High-Frequency to Low-Frequency Modes in Structures", *Journal of Vibration and Acoustics*, Vol. 117, Issue B, 1995, pp. 186,195.

[15] Weihua, S., and Cesnik, C., "Flight Dynamic Stability of a Flapping Wing Micro Air Vehicle in Hover", *Structural Dynamics and Materials Conference*, AIAA, 2011.

[16] Zhang, C., "Design and Control of Flapping Wing Micro Air Vehicles", Ph.D. Dissertation, Universidad Politecnica de Madrid, Spain, 2016.

[17] Schenato, L., Deng, X., and Sastry, S., "Hovering Flight for a Micromechanical Flying Insect: Modeling and Robust Control Synthesis", *IFAC Proceedings Volume*, Vol. 35, No. 1, 2002, pp. 235,240.

[18] Schenato, L., Deng, X., and Sastry, S., "Flapping Flight for Biomimetic Robotic Insects: Part II - Flight Control Design", *IEEE Transactions on Robotics*, Vol. 22, No. 4, 2006, pp. 789,803.

[19] Serrani, A., Keller, B., Bolender, M., and Doman, D., "Robust Control of a 3-DOF Flapping Wing Micro Air Vehicle", *AIAA Guidance, Navigation, and Control Conference*, AIAA, Vol. 7709, 2010.

[20] Chirarattananon, P., Ma, K.Y., and Wood, R. J., "Adaptive control for takeoff, hovering, and landing of a robotic fly", *International Conference on Intelligent Robots and Systems*, IEEE/RSJ, 2013

[21] Guo, Q., Minglang, H., Wei, R., Xu, J., and Song, H., "Hovering Control based on fuzzy neural networks for biomimetic flying robotic", *International Conference on Information and Automation*, ICIA, 2008.

[22] Balta, M., Ahmed, K. A., Wang, P. L., McCarthy, J. M., and Taha, H. E., "Design and Manufacturing of Flapping Wing Mechanisms for Micro Air Vehicle", *Structures, Structural Dynamics and Materials Conference*, AIAA, 2017, pp. 9,13.

[23] Hu, Z. and Deng, X., "Design and performance of insect inspired high frequency flapping wing robots," *Stainless steel*, Vol. 8, 2013, pp. 0,32.

[24] Breman, G.J., and Wang, Z.J., "Energy-minimizing kinematics in hvering insect flight", *Journal of Fluid Mechanics*, Vol. 528, 2007,pp. 153,168

[25] Wang, Z.J., Birch, J.M.m and Dickinson, M.H., "Unsteady forces in hovering flight:computation vs experiments", *Journal of Experimental Biology*, Vol 207, 2004, pp. 449,460.

[26] Taha, H.E., and Hassan, A.M., "Aerodynamic-Dynamic Interactions and Multi-Body Formulation of Flapping Wing Dynamics: Part 1 - Modeling", *AIAA Guidance, Navigation, and Control Conference*, AIAA, 2017.

[27] Taha, H.E., and Hassan, A.M., "Aerodynamic-Dynamic Interactions and Multi-Body Formulation of Flapping Wing Dynamics: Part 2 - Trim and Stability Analysis", *AIAA Guidance, Navigation, and Control Conference*, AIAA, 2017.

[28] Sarychev, A., "Stability Criteria for Time-periodic systems via high-order averaging techniques", *Nonlinear control in the year 2000*, Vol. 2, pp. 365,377.

[29] Ellington, C.P., "The aerodynamics of hovering insect flight. III. Kinematics", *Philosophical Transactions of the Royal Society*, Vol. 305, 1984, pp. 41,78.